Analyst

Accepted Manuscript

This article can be cited before page numbers have been issued, to do this please use: S. Shahrokhian and S. Ranjbar, *Analyst*, 2018, DOI: 10.1039/C8AN00725J.

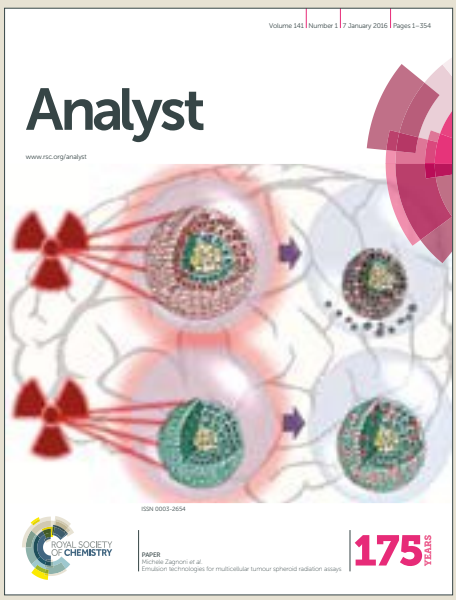

ROYAL SOCIETY OF CHEMISTRY

rsc.li/analyst

View Article Online
DOI: 10.1039/C8AN00725J

Aptamer Immobilization on Amino Functionalized Metal-Organic Frameworks: An Ultrasensitive Platform for Electrochemical Diagnostic of *Escherichia coli O157:H7*

Saeed Shahrokhian[1,2*], Saba Ranjbar[1]

[1]*Department of Chemistry, Sharif University of Technology, Tehran 11155-9516, Iran*

[2]*Institute for Nanoscience and Nanotechnology, Sharif University of Technology, Tehran, Iran*

Abstract. Here in, we developed an electrochemical biosensor for *Escherichia coli O157:H7* diagnostic based on amino-functionalized metal-organic frameworks (MOFs) as a new generation of organic-inorganic hybrid nanocomposites. Electrical and morphological properties of MOFs are enhanced by interweaving of each isolated MOF crystal with polyaniline (PANI). Subsequent attachment of amine modified aptamer to the polyanilinated MOFs is accomplished using glutaraldehyde (GA) as a cross linking agent. The prepared biocompatible platform is carefully characterized by means of field emission scanning electron microscopy (FESEM), energy dispersive spectroscopy (EDS), Fourier transform infrared spectroscopy (FT-IR) and X-ray powder diffraction (XRD) techniques. The biosensor fabrication and its electrochemical characterizations are monitored by cyclic voltammetry (CV) and electrochemical impedance spectroscopy (EIS) techniques. Differential pulse voltammetry (DPV) is applied to monitoring and quantitation of the interaction between aptamer and *E. coli O157:H7* using methylene blue (MB) as an electrochemical indicator. Changes in the reduction peak current of MB in the presence of *E. coli O157:H7* is recorded as an analytical signal and indicated a relationship with logarithm of the *E. coli O157:H7* concentration in the range of 2.1×10^{1} to 2.1×10^{7} CFU mL^{-1} with a LOQ of 21 CFU mL^{-1} and LOD of 2 CFU mL^{-1}. The electrochemical aptasensor displayed good recovery values for detection of *E. coli O157:H7* in environmental real samples and also can act as a smart device to investigate the effect of antibacterial agents against *E. coli O157:H7.*

Keywords: Metal-Organic Frameworks; Polyaniline; Electrochemical Biosensor; Pathogen Diagnostic; *Escherichia coli O157:H7*; Differential Pulse Voltammetry

*Corresponding author, Tel.: +98-21-66005718; Fax: +98-21-66002983.

E-mail address: shahrokhian@sharif.edu

View Article Online
DOI: 10.1039/C8AN00725J

1. Introduction

Accessing to the safe water reservoirs is one of the most important factors to define a developed country [1]. Pathogenic bacteria are most common water pollutant agents around the world, so that, more than 500 waterborne pathogen identified in drinking water by the US Environmental Protection Agency (EPA) [2]. In this context, the Crow Environmental Health Steering Committee (CEHSC) expressed its concern about direct relationship between water contamination and environmental contamination, food poisoning and outbreak of contagious diseases in the world [3]. Waterborne bacteria may cause a series of epidemic diseases including; abdominal cramps, vomiting and diarrhea and are great challenges for human health. According to World Health Organization (WHO), each year 3.4 million people, mostly children, die from water-related diseases (WHO 2014) [4].

Recently, to improved sanitation, measurement and management of water pathogen contaminations have been emphasized in many countries. Typical and standard methods [5-7] that are used for this purpose are accurate and reliable, but are consisted of specific enrichment media to separate, identify and count bacteria cell. Unfortunately, these processes take at least two-day after tedious sampling and preparation [8]. Accordingly, development of rapid and sensitive detection technologies is crucial for identification and quantitation of such pathogenic bacteria. Today, molecular recognition strategy has introduced and applied as a suitable method for direct assaying whole cell of pathogen. This strategy, named biosensing, is based on employing various molecular recognition elements (e.g. antibody [9], aptamer [10], polypeptide [11] and bacteriophage [12]) combined with mechanical, optical and electrochemical signal transductions [13, 14].

Among the possible biosensing technology, more attentions are focused on the aptamer-based biosensors due to some remarkable advantages (e.g. low cost in preparation, ease of

View Article Online
DOI: 10.1039/C8AN00725J

modification, high stability and acceptable specificity [15]). Aptamers are artificial single strands of DNA or RNA molecules with potential to binding to the specific targets by wrapping around it and formation of 3D structures [16]. Accordingly, in recent years considerable attentions have been devoted on design and fabrication of aptamer-based biosensors for detection of pathogen: *Salmonella typhimurium* [17], *Staphylococcus aureus*[18] , *Mycobacterium tuberculosis* [19], *Bacillus cereus* [20] and *Escherichia coli O157:H7* [21].

Taking advantages such as sensitivity, simplicity, portability and ease of preparation, make electronic devices as a valuable approach to integrate with recognition elements for developing electrochemical sensors and biosensors [22]. Different electrochemical methods including amperometry [23], potentiometry [24] and impedimetry [25] provide wide applications in the detection and quantitative determination of various biological and environmental targets in term of changes in electrical parameters. To achieve remarkable electrochemical performances, Nano-engineered materials have a great potential due to the improved sensitivity, stability and repeatability of the sensor's responses. In recent years, organic-inorganic hybrid nanocomposites have been extensively considered according to synergistic or complementary effects of their components [26]. Metal-organic frameworks (MOFs) are emerging as a new effective materials to modify the electrode surface in electrochemical applications. MOFs constructed by joining metal ions with organic linkers and are well-known due to their high porosity, effective surface area, thermal and chemical stabilities and tunable pore sizes [27] . Wide spread applications of MOFs are limited by their low conductivity and inappropriate water stability and dispersibility. In this regard, surface engineered MOFs have been developed according to the modification of host MOFs with guest nanomaterials (e.g. carbon nanostructures, metal nanoparticles and conductive polymers [28]). Nano engineered MOFs exhibit significant improvements in tunable conductivity,

View Article Online
DOI: 10.1039/C8AN00725J

surface morphology and electrocatalytic properties. Conductive polyaniline (PANI) have been developed as a promising candidate for this purpose, considering the impressive chemical and physical properties, environmental stability and excellent conductivity. On the other hand, in the biosensing field, PANI is regarded as an ideal matrix for the immobilization of biomolecules due to the presence of a large number of free $–NH_2$ functional groups in its structure [29, 30].

We report here, results of the studies related to design and fabrication of an effective electrochemical aptasensor based on PANI/MOFs for the direct detection of *Escherichia coli O157:H7* whole cell (a gram negative bacterium as a model) using DPV technique with methylene blue (MB) as a redox indicator. The $[Cu_3 (BTC)_2]$ metal-organic framework is easily synthesized from non-expensive and desired primary materials in moderate conditions. Moreover, the Cu-MOF was obtained in good yield and has a strong potential to be modified with the other nanomaterial to construction of Nano engineered metal-organic frameworks with high skeletal density. Large accessible –COOH groups in MOF structures make a better interaction with $–NH_2$ groups of PANI via carbodiimide chemistry. *E. coli O157:H7* detection can be realized by monitoring the changes of MB reduction peak current before and after incubation of aptasensor in *E. coli O157:H7* suspensions. Under optimum conditions, the designed strategy could be applied to sensitive and rapid detection of *E. coli O157:H7.* Also, we studied the selectivity, repeatability and applicability of the fabricated aptasensor in quantitative assessments in real samples.

2. Experimental

2.1. Chemicals and reagents

View Article Online
DOI: 10.1039/C8AN00725J

All chemical reagents with analytical grades including: copper(II) nitrate trihydrate, 1,3,5-benzenetricarboxylic acid (H_3BTC, 99%), aniline (99%), ammonium persulfate (APS), sodium borohydride, silver nitrate, trisodium citrate, sodium chloride, hydrochloric acid (HCl 37%), N-hydroxysuccinimide (NHS), N-(3-dimethylaminopropyl)-N-ethylcarbodimide hydrochloride (EDC), Glutaraldehyde (GA), Methylene blue (MB), Tris-HCl, potassium ferrocyanide, potassium ferricyanide, and ethanol were purchased from Merck. Aniline was distilled under vacuum and used as freshly prepared. But, the other chemicals were used as received without any further purification. The aqueous solutions were prepared using deionized water (DI, 18.2 MΩ in conductivity). Ampicillin trihydrate was obtained from Farabi pharmaceutical company (Tehran, Iran).

The $–NH_2$ modified *Escherichia coli O157:H7* aptamer were obtained from Bioneer Corporation (South Korea) and had the following sequence according to Cell-Systematic Evolution of Ligands by Exponential Enrichment (Cell-SELEX) process that reported in the literature [31]:

Escherichia coli O157:H7 aptamer sequences: 5′–NH_2 CCG GAC GCT TAT GCC TTG CCA TCT ACA GAG CAG GTG TGA CGG -3′

Stock solutions of DNA aptamers were prepared with the sterile distilled water (SD water) and stored at -20 ^{0}C when not they used.

All bacterial strains were obtained from microbial collection of Molecular Biology Department, National *E. coli* Reference Laboratory (NERL) of Pasteur Institute of Iran.

2.2. Instrumentation

View Article Online
DOI: 10.1039/C8AN00725J

The surface morphology and elemental composition of the synthesized materials were investigated using field emission scanning electron microscope (FE-SEM, MIRA3, TESCAN) equipped with an energy-dispersive X–ray spectroscopy (EDS) detector. X-ray powder diffraction (XRD) spectra were recorded on an X-ray diffractometer (GBC MMA) in the 2θ range from 5 to 90 using Cu Kα irradiation. The chemical structure information was obtained using Perkin Elmer FTIR spectrophotometer (spectrum 100) with a construction of KBr pellets. Size distribution of the prepared AgNPs was evaluated with Malvern Nano ZS (red badge) ZEN 3600 at the ambient temperature.

Optical density at 600 nm (OD 600) for estimation of the cultured bacteria and interaction of bacteria with AgNPs were obtained with a Perkin Elmer spectrophotometer (Lambda25).Optical microscope images were recorded with a fluorescence microscope (Nikon, Eclipse TE2000-S).

Electrochemical investigations including cyclic voltammetry (CV) and differential pulse voltammetry (DPV) were performed using a Metrohm potentiostat/galvanostat analyzer model 797VA. A three electrode system was used, including a glassy carbon working electrode (d=2.0 mm, Azar Electrode Co.), an Ag/AgCl (saturated KCl) reference electrode and a Pt wire auxiliary electrode. Cyclic Voltammograms (CVs) have been recorded at the scan rate of 100 mV s^{-1} and in the potential range between –0.2 to 0.6 V. Electrochemical impedance spectroscopy (EIS) measurements were performed with a Potentiostat/Galvanostat EG&G model 273A (Princeton Applied Research, USA) equipped with a Frequency Response Detector model 1025 (Power Suite software), which was used with a frequency between 5 kHz and 100 mHz and a 5 mV rms sinusoidal modulation under the open circuit potential (OCP) condition in the presence of a redox probe (0.1 M KCl containing 5 mM $Fe(CN)_6^{3-/4-}$). A digital pH/mV/ion meter

View Article Online
DOI: 10.1039/C8AN00725J

(Metrohm, pH Lab 827) was used for preparation of the buffer solutions. An ultrasonic bath (KODO model JAC 1002, Korea) was used for cleaning the electrodes surfaces and preparing the modifier suspensions.

2.3. Bacteria cultivation and plate counting of E. coli O157:H7

Escherichia coli O157:H7 and other bacteria strains used in this work were cultured in Luria-Bertani broth (LB) under shaking at 37 ^{0}C in an incubator during overnight. The optical density at 600 nm (OD 600) was recorded to estimate bacteria concentrations according to Mc Farland Turbidity Standard [32]. The enriched bacteria (estimated 2.1×10^9 CFU mL^{-1} for *E. coli O157:H7*) was centrifuged three times at 6000 rpm for 20 min (20 ^{0}C) and washed with PBS (0.1 M, pH = 7.4). Serial dilutions (2.1×10^8 to 2.1×10^0 CFU mL^{-1}) of *E. coli O157:H7* were prepared with sterile PBS and stored at 4 ^{0}C. It must be noted that, each experiment was performed under aseptic conditions.

Subsequently, 10^{-7} time dilution of *E. coli O157:H7* was coated in LB agar plate and incubated at 37 ^{0}C for 20 h. Finally *E. coli O157:H7* colonies on the plate were counted as a standard method.

2.4. Material preparation

2.4.1.Synthesis of AgNPs as an antibacterial agent

According to the litreture [33], AgNPs was synthesized in three steps. First, 250 µL of 100 mM $AgNO_3$ and 250 µL of 100 mM trisodium citrate were added to 100 mL of water. Then, 1 mL of 5 mM ice-cold $NaBH_4$ was added to above solution dropwise under vigorous stirring.

View Article Online
DOI: 10.1039/C8AN00725J

Finally, the resulted pale yellow solution was stirred for 30 min and stored at 4 ^{0}C in a dark place.

2.4.2. Synthesis of PANI/MOF as a modifier

Synthesis of $Cu_3(BTC)_2$ (HKUST-1)was performed according to previously reported paper [34]. In a typical procedure, 2.327 g of $Cu(NO_3)_2.3H_2O$ was dissolved in 25 mL DI water. The process was completed by addition of 50 mL solution including equal parts of ethanol and DI water containing 1.414 g H_3BTC. This mixture was completely dissolved and stirred for 15 min. the obtained solution was transferred into 250 mL Teflon-lined stainless steel autoclave at 130 ^{0}C for 15 h. Light blue crystals were obtained in this step that recovered by filtration and washing with water and ethanol. Finally, for activation of available –COOH groups as an effective binding site for appropriate interaction with $–NH_2$ groups of PANI, the synthesized $Cu_3(BTC)_2$ was dried under 60 ^{0}C for 12 h and then 10 mg of it was poured in 10 mL of 20 mM EDC/ 30 mM NHS (0.1 M PBS, pH = 7.4). Then, for removing the access amount of EDC/NHS, the activated MOF was centrifuged at 5000 rpm (10 min).

In following, the Cu-MOF/PANI nanocomposites were synthesized by in situ chemical oxidative polymerization according to previous paper [30] with some modifications. A 0.1 mL portion of the freshly distilled aniline monomer (99%) was added to HCl solution (4.9 mL, 0.1 M) and the mixture was sonicated for 5 min. Then 10 mg of the functionalized Cu-MOF (with EDC/NHS) was added to this mixture in an ice-bath under vigorous stirring.

In another glass breaker, 0.2 mg of $(NH_4)_2S_2O_8$ in 5 mL HCl 0.1M was prepared and once added to the above solution in an ice-bath under stirring condition. Next, resulting mixture was kept at room temperature for overnight without disrupting. After that, the obtained suspension

View Article Online
DOI: 10.1039/C8AN00725J

was centrifuged (5000 rpm, 10 min) and rinsed with DI water/ethanol for several times. At the end, the acquired product was dried at 60 ^{0}C for overnight. Also, pure PANI was synthesized by the same protocol without using Cu-MOF. The obtained PANI with this procedure has high conductive and has high specific surface area with a large population of free amine groups (–NH_2) that cause better immobilization of targets.

2.5. Aptasensor fabrication

At the first, the surface of glassy carbon electrode (GCE) was polished with alumina slurry (0.1 μM) on a polishing cloth, rinsed thoroughly with DI water and sonicated in ethanol for 5 min to remove unspecific adsorbed species. In the next, PANI/MOF/GCE was prepared with casting optimum volume of PANI/MOF suspension (4 μL) on the GCE surface and was dried in oven at 60 ^{0}C. The modified electrode was cycled between 0.0 to 1.0 V (vs. Ag/AgCl, with a scan rate of 100 mV s^{-1}) in PBS for five times. Then, 5 μL of glutaraldehyde (GA) aqueous solution (2.5%) was dropped at the surface of PANI/MOF/GCE and kept in a dark medium for 2h at room temperature. The prepared electrode was rinsed with DI water to remove unbounded GA. Finally, a 15 μL portion of amine-functionalized aptamer was incubated at the surface of GA/PANI/MOF/GCE overnight (Scheme. 1A). The –NH_2 groups of *E. coli O157:H7* specific aptamer are covalently attached to –NH_2 groups of PANI/MOF with GA as a cross linking agent. In fact, the porous structure of PANI/MOF provides a large accessible surface with lots of free amine groups for the immobilization of the aptamer. Before using the fabricated aptasensor, the prepared electrode was cycled in PBS (0.1 M, pH = 7.4) for five times.

2.6. Electrochemical detection

View Article Online
DOI: 10.1039/C8AN00725J

Electrochemical detection of *E. coli O157:H7* was performed using DPV in the potential range -0.5 to 0.2 V (vs. Ag/AgCl) at pulse amplitude of 50 mV using MB as a redox indicator. First, biosensor based on Apt/GA/PANI/MOF/GCE was incubated in 20 mM Tris-HCl (containing 20 µM MB and 20 mM NaCl) in 20 min as optimum condition and then washed with DI water to remove unbounded and non-specific adsorbed MB. The DPV signal of the intercalated MB on the aptamer at the surface of Apt/GA/PANI/MOF/GCE was recorded in PBS (0.1 M, pH = 7.4). In order to assure that nonspecific adsorbed MB and also PBS buffer have no significant effect in DPV response of the aptasensor for the *E. coli O157:H7* detection, the corrected signals obtained by immersing the aptasensor in pure PBS (0.1 M, pH = 7.4) without *E. coli O157:H7* for the certain time equal to MB incubation time. So, the DPV signal was recorded as an initial MB peak current (Fig. S1, Supplementary information).

In the next, the aptasensor containing intercalated MB was incubated in *E. coli O157:H7* suspension in the optimum condition. By interaction of the aptamer with specific epitopes at the *E. coli O157:H7* cell wall, the aptamer conformation was changed and MB released from the aptasensor. Analytical signal was calculated based on MB peak current change (ΔI_p) before and after presence of *E. coli O157:H7* (Scheme. 1B).

$$\Delta I_p = I_{p,\,MB}\,(\text{Aptamer - PBS}) - I_{p,\,MB}\,(\text{Aptamer - } \textit{E. coli O157:H7})$$

Scheme. 1

2.7. Virtual simulations

Virtual simulations provide an outstanding tool to predict the interaction of biological molecules. This process allowed us to obtain the beneficial information about binding sites, biomolecule complex, constant formation and molecule-molecule interactions. In this study, secondary structure of aptamer and specific binding with some epitopes at outer cellular

View Article Online
DOI: 10.1039/C8AN00725J

membrane of *E. coli O157:H7* was predicted with mfold and HEX.8.0.0 software and depicted in Figs. S2 and S3.

2.8. Antibacterial test

The effect of two antibacterial agents including ampicillin as an antibiotic drug and AgNPs against *E. coli O157:H7* was evaluated with fabricated aptasensor. For this purpose, 10 µL of *E. coli O157:H7* (2.1×10^9 CFU mL^{-1}) was added to 990 µL of ampicillin (1mM) and AgNPs separately to final concentration of 2.1×10^7 CFU mL^{-1}. After incubation of *E. coli O157:H7* with these antibacterial agents for 24h, electrochemical signals of the aptasensor were recorded with DPV, CV and EIS techniques and confirmed with the data from optical microscope and UV-Vis spectrophotometer.

2.9. Real sample preparation

In order to investigate applicability of the fabricated aptasensor in real samples, some water samples were obtained from different source and spiked with *E. coli O157:H7* to final concentration 2.1×10^3 CFU mL^{-1}. The water samples containing *E. coli O157:H7* were analyzed using the electrochemical assay following the steps described in section 2.6.

3. Results and discussion

3.1. Physicochemical characterization of the prepared modifier

The surface structure and morphology of the prepared modifier was obtained with FESEM images and bulk composition examined with EDS analysis. The SEM images of $Cu_3(BTC)_2$ exhibited pyramidal crystalline structures with particle sizes about 5-15 µm (Fig. 1A). Also, the

View Article Online
DOI: 10.1039/C8AN00725J

EDS analysis confirmed the presence of C, Cu and O in the structure of the synthesized MOFs. Fibrous morphology with a large number of interconnected tubules with an agglomerated structure was obtained for PANI according to SEM images (Fig. 1B), and presence of C, N, S and Cl confirmed in the backbone of the conducting polymer with EDS analysis. As can be seen in Fig. 1C, after the polymerization of MOF, compressed chains of PANI covered the surface of MOF and a cauliflower-like structure is obtained for PANI/MOF. In fact, each isolated MOF crystal is interconnected with the others and PANI can act as a conductive bridge between MOF crystals for electron transportation during the system. The EDS pattern revealed an evidence for existence of C, N, Cu, S and Cl in the structure of PANI/MOF. Also, reduction of the amount of Cu from 12.55 w% to 0.1 w% in PANI/MOF compared to MOF proved that the surface of MOF completely covered with PANI. The data of EDS analysis is shown in Fig. S4.

With comparison the SEM images of PANI and PANI/MOF (Figs. 1B & 1C), it's cleared that presence of MOF creates a porous and non-smooth structure for the immobilization of more amount of the target.

Fig. 1

The crystal structure of MOF, PANI and PANI/MOF was confirmed by X-ray powder diffraction (XRD) and is shown in Fig. 2A. Several well-defined sharp peaks for MOF in the XRD pattern indicated a highly crystalline microporous structure for it. 2θ values of 5.84°, 9.51°, 11.65°, 13.5°, 19.81°, 25.33° and 29.37° represent the planes of (200), (220), (222), (440), (400), (040) and (201), respectively, and show a good agreement with the literature [35] for Cu-MOF. The XRD pattern for PANI exhibits three broad diffraction peak at 2θ values of 15.09°, 20.37° and 25.35° related to (011), (020) and (200) planes [30]. Finally, the PANI/MOF composite showed a similar diffraction pattern to pure PANI with disappearance of the sharp diffraction peaks of

View Article Online
DOI: 10.1039/C8AN00725J

MOF. This observation suggested that the amorphous structure of PANI effectively covered the surface of crystalline MOF, due to the formation of a core-shell structure.

The structural information about the synthesized materials was obtained using Fourier transform infrared spectra (FT-IR) in the range of 500-4000 cm^{-1} and results are presented in Fig. 2B. FT-IR analysis confirmed the presence of Cu-O stretching vibration (488, 730 cm^{-1}), symmetric stretching of carboxylate ion (1372, 1447 cm^{-1}), asymmetric stretching of carboxylate ion (1567, 1643 cm^{-1}), C=O stretching vibration (1706 cm^{-1}) and O-H stretching vibration peaks of ethanol and water (3425 cm^{-1}). Also, the FT-IR results for pure PANI indicated several main peaks in 1075, 1291, 1472 and 1547 cm^{-1} that are attributed to N=Q=N stretching (Q is quinonoid ring), C-N stretching vibration and C=C stretching of benzenoid and quinonoid ring, respectively. Especially the peak between 2500-3500 cm^{-1} are due to =N-H stretching vibration. From the FT-IR spectrum for PANI/MOF, it can be found that PANI/MOF has similar characteristic peaks of PANI implying that they have similar molecular structure [36].

Fig. 2

3.2. Electrochemical characterization of designed aptasensor

Cyclic voltammetry (CV) and electrochemical impedance spectroscopy (EIS) are powerful techniques that have a great potential to monitor the electrode surface in each step of the biosensor fabrication. The detailed principle of cyclic voltammograms (CVs) and Nyquist plots of the purposed aptasensor in the presence of a redox probe (0.1 M KCl containing 5 mM $Fe(CN)_6^{3-/4-}$) are depicted in Fig. 3. Results indicated that, a remarkable decrease in the redox peak current together with an increase in the charge transfer resistance (R_{ct}) obtained for GCE after modification with Cu-MOF due to its non-conductivity characteristics. But, a great

View Article Online
DOI: 10.1039/C8AN00725J

enhancement in the conductivity for MOF obtained after the polymerization of PANI that leads to increasing of the redox peak current and decreasing the R_{ct}. After dropped GA as a cross linking agent, packed imine adhesion layer was formed at the surface of PANI/MOF/GCE and electron transfer of redox probe was disrupted. Actually, formation of covalent bonds between GA and NH_2 groups of PANI is responsible of these changes. The CV and Nyquist plot were applied to investigate the effect of GA and the results are shown in Fig. S5 by detailed. The schematic illustration of the interaction of GA with PANI and amine functionalized aptamer is shown in Scheme S1.

In following, the redox peak current was decreased and R_{ct} increased after immobilization of aptamer at the surface of GA/PANI/MOF/GCE. These were the results of negative charge of phosphate group in the aptamer backbone that repelled the electron transfer of probe at the surface of electrode. These trends were continued with incubation of aptasensor in 2.1×10^7 CFU mL^{-1} of *E. coli O157:H7* suspension that leads to formation of aptamer- *E. coli O157:H7* complex and create steric hindrance for diffusion of redox probe to the electrode surface.

Fig. 3

GA and MOF are two key components in the aptasensor fabrication. The main role of MOFs is to create a porous structure with high surface area to immobilize more amounts of the aptamer. The influence of MOF was evaluated using Apt/GA/PANI/GCE. The results indicated that, the value of MB peak current is low due to less amount of the immobilized aptamer at the surface of GA/PANI/GCE (Figs. S6A and S6B). Also, the effect of cross linking agent was investigated with elimination of GA from the aptasensor fabrication procedure [37]. Here in, aptamer was directly immobilized at the surface of PANI/MOF/GCE and DPV signal of 20 μM MB was recorded. The results indicated that, in the absence of GA, interaction of PANI and

View Article Online
DOI: 10.1039/C8AN00725J

amine modified aptamer is not established very well. Therefore, insufficient amount of aptamer can immobilize at the surface of PANI/MOF/GCE and less amount of MB intercalated with aptasensor. Then, MB peak current and its corresponding change are insignificant in this case (Figs. S6C and S6D).

3.3. Optimization of experimental parameters

To achieve the best performance for *E. coli O157:H7* detection, various experimental parameters including modifier thickness, indicator conditions and *E. coli O157:H7* incubation time was optimized.

3.3.1. Modifier thickness

In order to improve the aptasensor response, thickness of the modifier on GCE surface was investigated. The modifier film thickness was controlled by casting the various volumes of PANI/MOF suspension (1-5 μL). The results indicated that the best electrode response to immobilization of aptamer and capture of 2.1×10^4 CFU mL^{-1} *E. coli O157:H7* was observed by casing 4 μL of the modifier suspension on the surface of GCE (Fig. S7).

3.3.2. Indicator parameters

To maximize the efficiency and sensitivity of the aptasensor response, the concentration and incubation time of MB as an indicator were optimized. According to Fig. S8, the peak current of MB increased by increasing the incubation time from 0 to 20 min and reached a plateau after 20 min. In this time the most MB molecules have intercalated with ss-DNA of the

View Article Online
DOI: 10.1039/C8AN00725J

aptamer. Therefore, maximum peak current for MB obtained and 20 min was chosen as optimum incubation time of MB.

Also, the influence of MB concentration (20, 50 and 100 μM) was studied and the best results obtained for 20 μM MB as an optimum indicator concentration (Fig. S9).

3.3.3. *E. coli O157:H7 incubation time*

The effect of binding time between the aptamer and *E. coli O157:H7* was evaluated based on decreasing MB peak current in the presence of *E. coli O157:H7.* By increasing the incubation time of the aptasensor in 2.1×10^4 CFU mL^{-1} of *E. coli O157:H7* suspension until 20 min, significant decrease in MB peak current observed due to specific interaction between aptamer and *E. coli O157:H7* and releasing of MB from the aptasensor. After this time, no significant change was observed and therefore, 20 min set as optimum *E. coli O157:H7* incubation time (Fig. S10).

3.4. Analytical figures of merit

After characterization of Apt/GA/PANI/MOF and optimization of the experimental parameters, the analytical performance of the aptasensor was evaluated. The calibration curve was obtained based on the change in the MB peak current with incubation of aptasensor in MB, PBS and (2.1×10^0 to 2.1×10^9 CFU mL^{-1}) *E. coli O157:H7* suspension followed by section 2.6. As can be seen in Fig. 4, the linear relationship between ΔI_p and logarithm of *E. coli O157:H7* concentration was obtained for 2.1×10^1 to 2.1×10^7 CFU mL^{-1} followed by LOQ of 21 CFU mL^{-1} and LOD of 2 CFU mL^{-1} (each experiment was three times repeated and LOD was determined by $3S_b/m$, S_b is the blank standard deviation and m is the slope of the calibration curve).

View Article Online
DOI: 10.1039/C8AN00725J

Fig. 4

It also found that, the fabricated aptasensor could be easily regenerated during 1-5 cycles by dissociating *E. coli O157:H7* (2.1×10^4 CFU mL^{-1}) from the aptamer in 2M NaCl for 1h (data shown in Fig. S11). At the first cycle of the regeneration process, the MB peak current was decreased after incubation of *E.coli O157:H7*/MB/Apt/GA/PANI/MOF/GCE in 2M NaCl. We assume that, this observation is due to releasing of some weakly bonded aptamers in addition to *E.coli O157:H7* at the surface of GA/PANI/MOF/GCE in salt medium. This manner was not observed at 2-5 next cycles and MB peak current at the surface of Apt/GA/PANI/MOF/GCE reached to a similar constant value. In the other hand, the aptasensor achieved the stable conditions after the first cycle.

Moreover, durability of the modifier film during the regeneration process is proved by SEM images. The morphology of the electrode surface before sensing and after regeneration showed to be same and no obvious difference was observed during the regeneration process. Also, the SEM investigations showed that after the incubation of aptasensor in *E. coli O157:H7* suspension, the bacteria that captured by aptamers can be observed at the surface of the electrode (Fig. 5).

The precision of the fabricated aptasensor was estimated by measuring the MB peak current of five replicate for an aptasensor (a same modified electrode) in PBS (as the blank), 2.1×10^2 CFU mL^{-1} and 2.1×10^6 CFU mL^{-1} concentration of *E. coli O157:H7*. The resulting relative standard deviation (RSD) values were 6.01%, 4.1% and 5.4%, indicating acceptable precisions for the designed strategy. Moreover, the reproducibility of the aptasensor response was determined by applying five different aptasensor, which were fabricated with the same

View Article Online
DOI: 10.1039/C8AN00725J

procedure for the blank and mentioned concentration of *E. coli O157:H7*. The calculated RSD values during these experiments were 6.51%, 6.34% and 6.52%.

In the following, the stability of the fabricated aptasensor was evaluated by storing the prepared aptasensor in 4 ^{0}C over a period of two weeks. The results indicated that the electrochemical response of aptasensor decreased only slightly and retained 90% of its initial response for 2.1×10^{6} CFU mL^{-1} of *E. coli O157:H7*.

The selectivity of the aptasensor response was studied by incubation of MB/Apt/GA/PANI/MOF/GCE in 2.1×10^{7} CFU mL^{-1} of five other bacteria including: *Escherichia coli E23, Escherichia coli DH5α, Staphylococcus aureus, Salmonella typhimurium* and *Pseudomonas aeruginosa*. From the results in Fig. S12, it could be realized that changes in the MB peak current in the presence of other bacteria is much lower than *Escherichia coli O157:H7.* The comparison of this method with other similar analytical methods is summarized in Table. S1[24, 37-40]. The fabricated aptasensor have a potential to detect *E. coli O157:H7* in a wide linear dynamic range with seven orders of magnitude that makes analysis (especially for analysis of real samples) faster and simpler by avoiding re-assays and dilution issues.

3.5. Method validation

The performance of the purposed aptasensor was compared with colony plate counting as the standard reference method. A 10^{-7} time dilution of *E. coli O157:H7* was coated in LB agar plate. After incubation of plate at 37 ^{0}C for 20 h, the cultured colony was counted and an average 255 CFU mL^{-1} calculated based on 3 times repetition (Fig. S13). The relative error for the response of the fabricated aptasensor, compared with the standard method, was calculated 17.65%.

View Article Online
DOI: 10.1039/C8AN00725J

3.6. *Antibacterial test*

A systematic and detailed study of antibacterial agents was performed against *E. coli O157:H7* in the presence of ampicillin (as an antibacterial drug) and AgNPs.

First, the synthesized AgNPs was characterized with FESEM and EDS analysis (Fig. S14) and indicated monodispersed spherical shape. In the next, antibacterial effect of these agents was evaluated using CV, DPV and EIS techniques and confirmed with optical microscope images. Then, UV-Vis spectrophotometry and DLS analysis were performed to investigation of AgNPs-*E. coli O157:H7* interaction.

Antibacterial agents can disrupt the target cell with adhesion to the cell wall and penetrate to the membrane for damage the structural integrity and physicochemical properties of bacteria. In fact, antibacterial agents may cause inactivation of *E. coli O157:H7* with formation of pits/hole on the cell wall, inhibition of DNA replication and generation of reactive oxygen species (ROS) [41].

Accordingly, after incubation of *E. coli O157:H7* with antibacterial agents, the outer membrane with accessible epitopes (proteins, peptidoglycan, lipoprotein, lipopolysaccharide and acids) was damaged and interaction of the aptamer and *E. coli O157:H7* was disrupted [42]. So, aptamer is not able to wrap around the specific epitopes of bacteria and aptasensor can't capture the antibacterial treated *E. coli O157:H7* like untreated *E. coli O157:H7.* As can be seen in Fig. 6A, decreasing of the MB peak current in aptasensor for the dead *E. coli O157:H7* (treated with both AgNPs and ampicillin) is very weak. However, significant decrease in MB peak current was observed in the presence of live bacteria. In support of the above results, CV and EIS were recorded for both untreated and treated *E. coli O157:H7.* In comparison to untreated *E. coli*

View Article Online
DOI: 10.1039/C8AN00725J

*O157:*H7, in the presence of antibacterial treated *E. coli O157:H7* changes in redox peak current and charge transfer resistance of aptasensor (in presence of a redox probe 0.1 M KCl containing 5 mM $Fe(CN)_6^{3-/4-}$) are negligible (Fig. 6 B and C).

Fig. 6

On the other hands, the results obtained by optical microscope have a good agreement with the electrochemical sensing tests. According to Fig. S15, the treated *E. coli O157:H7* with antibacterial agents cause to shrinkage of *E. coli O157:H7* cell wall, while, untreated cell appeared in normal and characteristic shape.

It must be noted that, addition of *E. coli O157:H7* suspension to AgNPs led to the aggregation of AgNPs at 24 h (Scheme. 2). Aggregation of AgNPs in the presence of *E. coli O157:H7* was followed by naked eyes and UV-Vis spectrophotometry (Fig. 7). During this process, the color of solution changes from light yellow to dark yellow and oranges with a red shift in the absorption spectra. The UV-Vis absorption spectrum of AgNPs indicated a characteristic peak at 400 nm. But after addition of *E. coli O157:H7*, this peak was decreased and a new broad absorption band was appeared around 545 nm.

The aggregation of AgNPs was supported with DLS analysis, which showed that monodispese AgNPs (30-60 nm) aggregated irregularly to form large clusters (700-800 nm) in the presence of *E. coli O157:H7*. Corresponding data are shown in Fig. S16.

Scheme. 2

Fig. 7

3.7. Real sample analysis

View Article Online
DOI: 10.1039/C8AN00725J

To evaluate the accuracy of the developed method, the fabricated aptasensor was used for recovery tests in different water samples. The water samples were spiked with 2.1×10^3 CFU mL^{-1} of *E. coli O157:H7* and recoveries obtained for different samples (73.2-113.6 %). The results in Table S2 confirmed the acceptable potential and feasibility of the fabricated aptasensor for simple, accurate and fast determination of *E. coli O157:H7* in real samples.

Conclusions

Since pathogenic bacteria have serious effects in the public health, environment and food supplies, so, fast and accurate diagnostic of them is high demanded recently. In present study, we address this challenge by provide a novel electrochemical biosensor based on amino functionalized metal-organic frameworks integrated with an aptamer as a sensing element. Due to the advantages of sensitivity, selectivity, fast responsibility and reliability, the fabricated aptasensor enable us to detect and determine of *E. coli O157:H7* in a wide linear dynamic range with a low limit of detection in real samples. Also, the purposed aptasensor have been successfully applied as an ultrasensitive device to evaluate the effect of antibacterial agents against *E. coli.*

Acknowledgments

The authors gratefully acknowledge the support of this work by the Research Council and the Center of Excellent for Nanostructures of Sharif University of Technology, Tehran, Iran (Grant No. G930616). And also, the authors are thankful to Dr. Mana Oloomi from Department of Molecular Biology, Pasteur Institute of Iran.

View Article Online
DOI: 10.1039/C8AN00725J

References

1. P. K. Pandey, P. H. Kass, M. L. Soupir, S. Biswas and V. P. Singh, *AMB Express*, 2014, **4**, 51.
2. N. J. Ashbolt, *Curr. Environ. Health Rep.*, 2015, **2**, 95-106.
3. C. L. Richards, S. C. Broadaway, M. J. Eggers, J. Doyle, B. H. Pyle, A. K. Camper and T. E. Ford, *Microb. Ecol.*, 2015, 1-12.
4. N. Reta, C. P. Saint, A. Michelmore, B. Prieto-Simon and N. H. Voelcker, *ACS App. Mater. Interfaces*, 2018, 10 (7), 6055-6072.
5. J. Pires, A. Novais and L. Peixe, *J.Clin. Microbiol.*, 2013, **51**, 4281-4283.
6. A. Witt, M. J. Mason, K. Burgess, S. Flocke and S. Zyzanski, *Breastfeed. Med.*, 2014, **9**, 29-34.
7. P. Elizaquível, G. Sánchez and R. Aznar, *Food Control*, 2012, **25**, 704-708.
8. A. Hematian, N. Sadeghifard, R. Mohebi, M. Taherikalani, A. Nasrolahi, M. Amraei and S. Ghafourian, *Osong public health and Res. perspectives*, 2016, **7**, 77-82.
9. G. Vásquez, A. Rey, C. Rivera, C. Iregui and J. Orozco, *Biosens. Bioelectron.*, 2017, **87**, 453-458.
10. H. Shen, J. Wang, H. Liu, Z. Li, F. Jiang, F.-B. Wang and Q. Yuan, *ACS App. Mater. Interfaces*, 2016, **8**, 19371-19378.
11. E. Tenenbaum and E. Segal, *Analyst*, 2015, **140**, 7726-7733.
12. N. Bhardwaj, S. K. Bhardwaj, J. Mehta, K.-H. Kim and A. Deep, *ACS App.Mater. Interfaces*, 2017, **9**, 33589-33598.
13. S. Shahrokhian, R. Salimian and H. R. Kalhor, *RSC Adv.*, 2016, **6**, 15592-15598.
14. J. Chen, S. M. Andler, J. M. Goddard, S. R. Nugen and V. M. Rotello, *Chem. Soc. Rev.*, 2017, **46**, 1272-1283.
15. R. Nezlin, *Mol. Immunol.*, 2016, **70**, 149-154.
16. I. Jeddi and L. Saiz, *Sci. Rep.*, 2017, **7**, 1178.
17. S. Ranjbar, S. Shahrokhian and F. Nurmohammadi, *Sens. Actuators B*, 2018, **255**, 1536-1544.
18. S. Ranjbar and S. Shahrokhian, *Bioelectrochem.,* 2018, **123**, 70-76.
19. C. Liu, D. Jiang, G. Xiang, L. Liu, F. Liu and X. Pu, *Analyst*, 2014, **139**, 5460-5465.
20. Z. Izadi, M. Sheikh-Zeinoddin, A. A. Ensafi and S. Soleimanian-Zad, *Biosens. Bioelectron.*, 2016, **80**, 582-589.
21. S. Chen, X. Chen, L. Zhang, J. Gao and Q. Ma, *ACS Appl. Mater. Interfaces*, 2017, **9**, 5430-5436.
22. C. Zhu, G. Yang, H. Li, D. Du and Y. Lin, *Anal. Chem.*, 2014, **87**, 230-249.
23. Z. Liu, H. Forsyth, N. Khaper and A. Chen, *Analyst*, 2016, **141**, 4074-4083.
24. G. A. Zelada-Guillén, J. Riu, A. Düzgün and F. X. Rius, *Angew. Chem. Int. Ed.*, 2009, **48**, 7334-7337.
25. A. D. Chowdhury, A. De, C. R. Chaudhuri, K. Bandyopadhyay and P. Sen, *Sens. Actuators*, 2012, **171**, 916-923.
26. G. Maduraiveeran and W. Jin, *Trends Environ. Anal. Chem.*, 2017, **13**, 10-23.
27. E. Asadian, S. Shahrokhian and A. I. Zad, *J. Electroanal. Chem.*, 2018, **808**, 114-123.
28. T. Kitao, Y. Zhang, S. Kitagawa, B. Wang and T. Uemura, *Chem. Soc. Rev.*, 2017, **46**, 3108-3133.

View Article Online
DOI: 10.1039/C8AN00725J

29. L. Wang, X. Feng, L. Ren, Q. Piao, J. Zhong, Y. Wang, H. Li, Y. Chen and B. Wang, *J. Am. Chem. Soc.*, 2015, **137**, 4920-4923.
30. S. Guo, Y. Zhu, Y. Yan, Y. Min, J. Fan, Q. Xu and H. Yun, *J. Power Sources*, 2016, **316**, 176-182.
31. W.-h. Wu, M. Li, Y. Wang, H.-x. Ouyang, L. Wang, C.-x. Li, Y.-c. Cao, Q.-h. Meng and J.-x. Lu, *Nanoscale Res. Lett.*, 2012, **7**, 658-664.
32. J. McFarland, *J. Am. Med. Assoc.* 1907, **49**, 1176-1178.
33. Z. J.-N. Ivrigh, N. Fahimi-Kashani and M. R. Hormozi-Nezhad, *Spectrochim. Acta A,* 2017, **187**, 143-148.
34. J.-B. Raoof, S. R. Hosseini, R. Ojani and S. Mandegarzad, *Energy*, 2015, **90**, 1075-1081.
35. D. Y. Lee, D. V. Shinde, S. J. Yoon, K. N. Cho, W. Lee, N. K. Shrestha and S.-H. Han, *J. Phys. Chem. C*, 2013, **118**, 16328-16334.
36. K. E. Ramohlola, G. R. Monana, M. J. Hato, K. D. Modibane, K. M. Molapo, M. Masikini, S. B. Mduli and E. I. Iwuoha, *Composites Part B: Engineering*, 2018, **137**, 129-139.
37. N. Hao, X. Zhang, Z. Zhou, R. Hua, Y. Zhang, Q. Liu, J. Qian, H. Li and K. Wang, *Biosens. Bioelectron.*, 2017, **97**, 377-383.
38. S. Brosel-Oliu, R. Ferreira, N. Uria, N. Abramova, R. Gargallo, F.-X. Muñoz-Pascual and A. Bratov, *Sens. Actuators B*, 2018, **255**, 2988-2995.
39. H. Huang, M. Liu, X. Wang, W. Zhang, D.-P. Yang, L. Cui and X. Wang, *Nanoscale Res. Lett.*, 2016, **11**, 507.
40. M. B. Dos Santos, J. Agusil, B. Prieto-Simón, C. Sporer, V. Teixeira and J. Samitier, *Biosens. Bioelectron.*, 2013, **45**, 174-180.
41. S. Agnihotri, S. Mukherji and S. Mukherji, *Rsc Adv.*, 2014, **4**, 3974-3983.
42. J. Duan, H. Yin, R. Wei and W. Wang, *Biosens. Bioelectron.*, 2014, **57**, 139-142.

View Article Online
DOI: 10.1039/C8AN00725J

FIGURES CAPTIONS

Scheme 1. Schematic illustration of (A) aptasensor fabrication and (B) *E. coli O157:H7* detection.

Scheme 2. Schematic representation of the AgNPs aggregations in presence of *E. coli O157:H7.*

Fig. 1 FESEM images of (A) Cu-MOF, (B) PANI and (C) PANI/MOF.

Fig. 2 (A) XRD pattern and (B) FTIR spectra of (a) Cu-MOF, (b) PANI and (c) PANI/MOF.

Fig. 3 (A) Cyclic voltammograms (Scan rate, 100 mVs^{-1}) and (B) Nyquist plots of 0.1 M KCl containing 5 mM $Fe(CN)_6^{3-/4-}$ in each steps of aptasensor fabrication for *E. coli O157:H7* detection.

Fig. 4 (A) DPV responses in presence of Tris-HCl (20 mM, pH 7.4) containing 20 μM of MB for different concentrations (2.1×10^7-2.1×10^1 CFU mL^{-1}) of *E. coli O157:H7*, (B) corresponding linear calibration curve of ΔI_p versus logarithm of *E. coli O157:H7* concentration.

Fig. 5 The SEM images of Apt/GA/PANI/MOF/GCE (A) before sensing, (B) after sensing *E. coli O157:H7* and (C) after regeneration in presence of 2M NaCl.

Fig. 6 (A) DPV signal of 20 μM MB (in 20 mM Tris-HCl, pH 7.4), (B) Cyclic voltammograms and (C) Nyquist plots in presence of 0.1 M KCl containing 5 mM $Fe(CN)_6^{3-/4-}$ for (a) aptasensor, aptasensor incubated in (b) 2.1×10^6 CFU mL^{-1} *E. coli O157:H7*, (c) AgNPs treated *E. coli O157:H7* (2.1×10^6 CFU mL^{-1}) and (d) ampicillin treated *E. coli O157:H7* (2.1×10^6 CFU mL^{-1}).

Fig. 7 Absorption spectra and color solution of (a) monodispersed AgNPs and (b) aggregated AgNPs in presence of *E. coli O157:H7* after 24h.

View Article Online
DOI: 10.1039/C8AN00725J

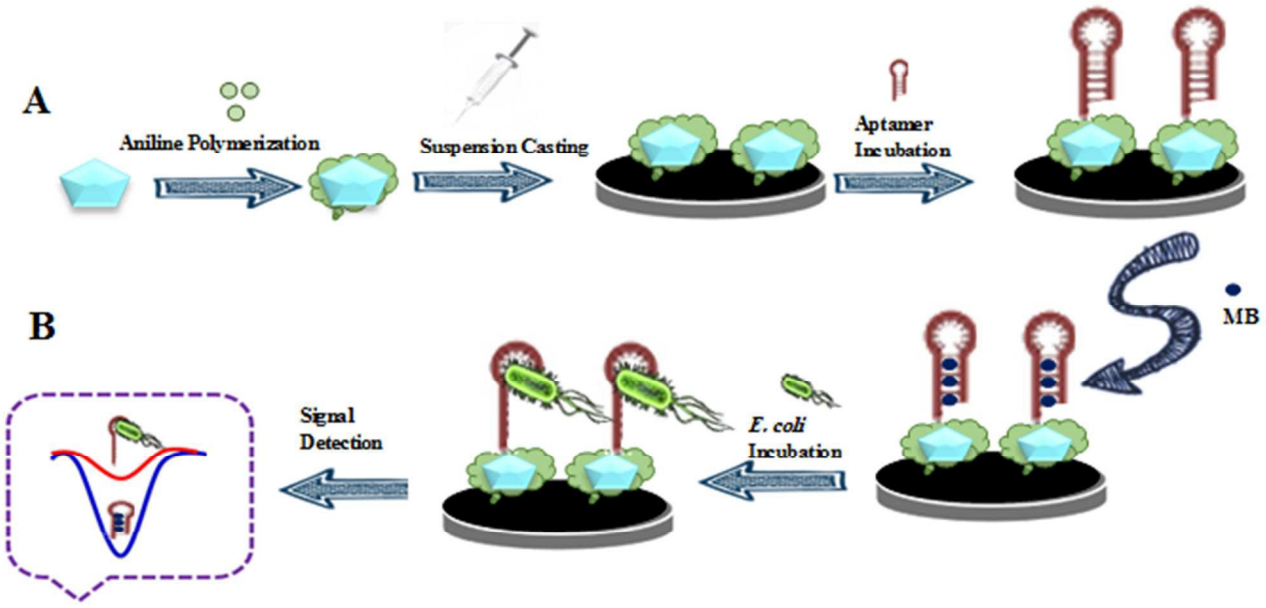

Scheme1

View Article Online
DOI: 10.1039/C8AN00725J

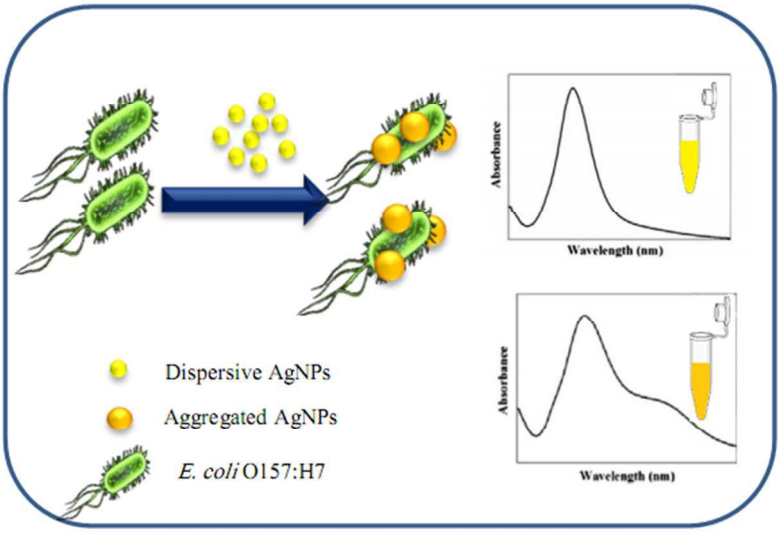

Scheme2

View Article Online
DOI: 10.1039/C8AN00725J

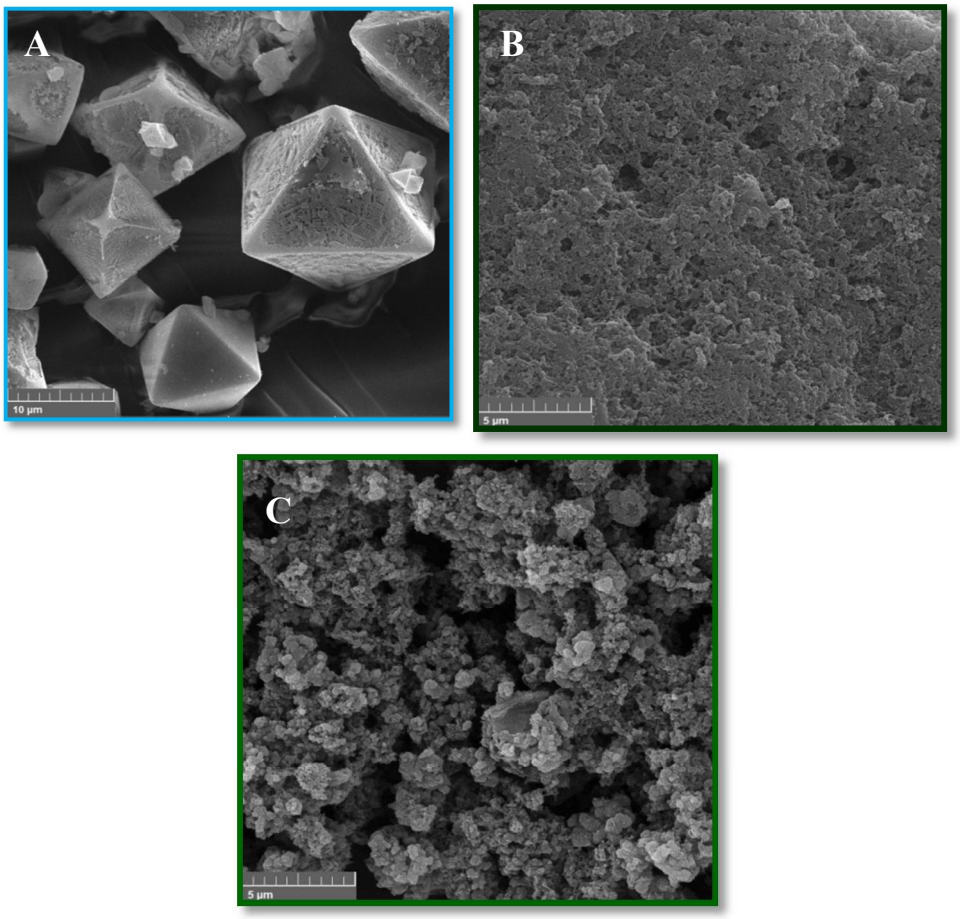

Fig. 1

View Article Online
DOI: 10.1039/C8AN00725J

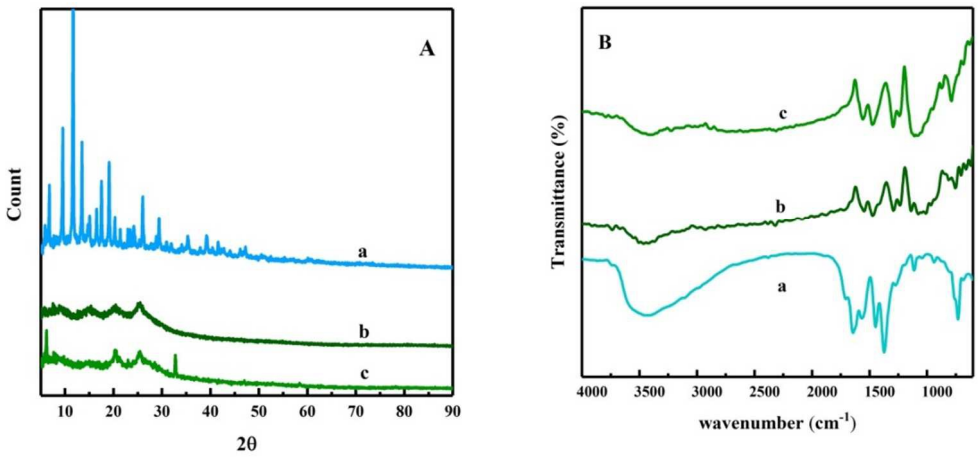

Fig. 2

View Article Online
DOI: 10.1039/C8AN00725J

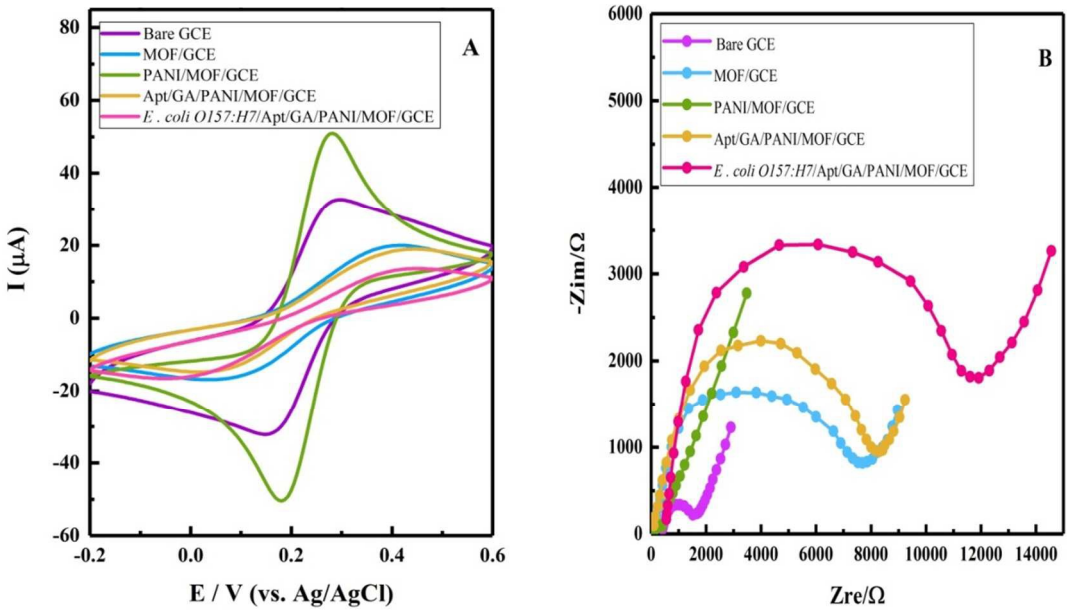

Fig. 3

View Article Online
DOI: 10.1039/C8AN00725J

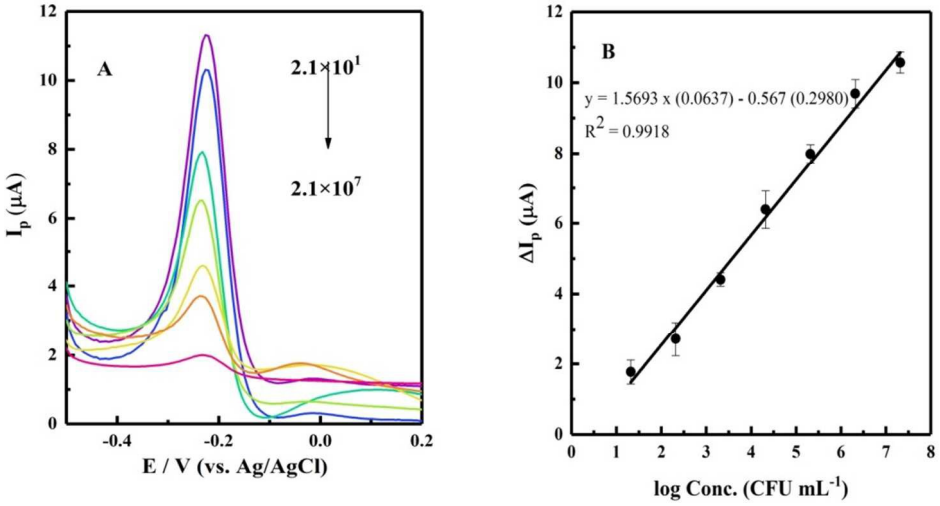

Fig. 4

View Article Online
DOI: 10.1039/C8AN00725J

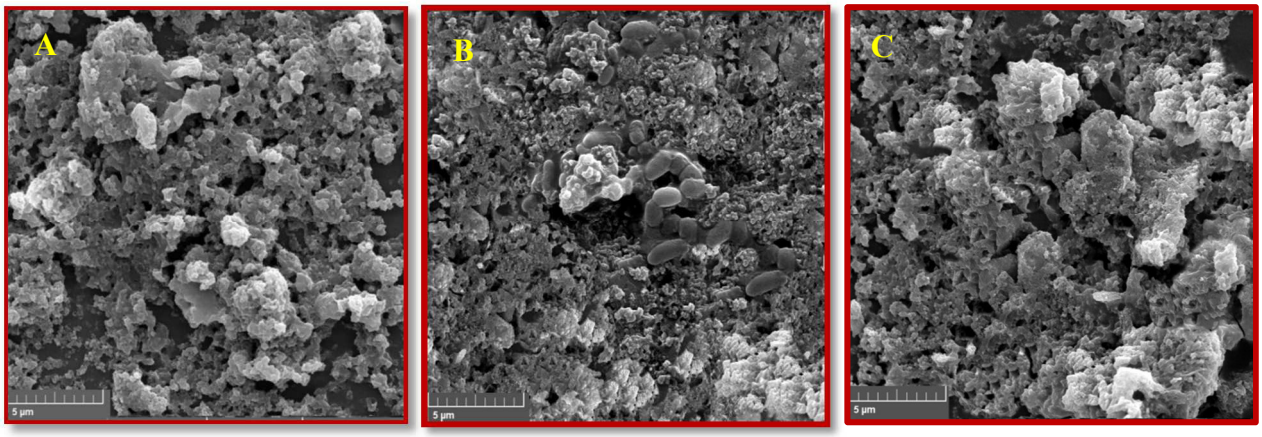

Fig. 5

View Article Online
DOI: 10.1039/C8AN00725J

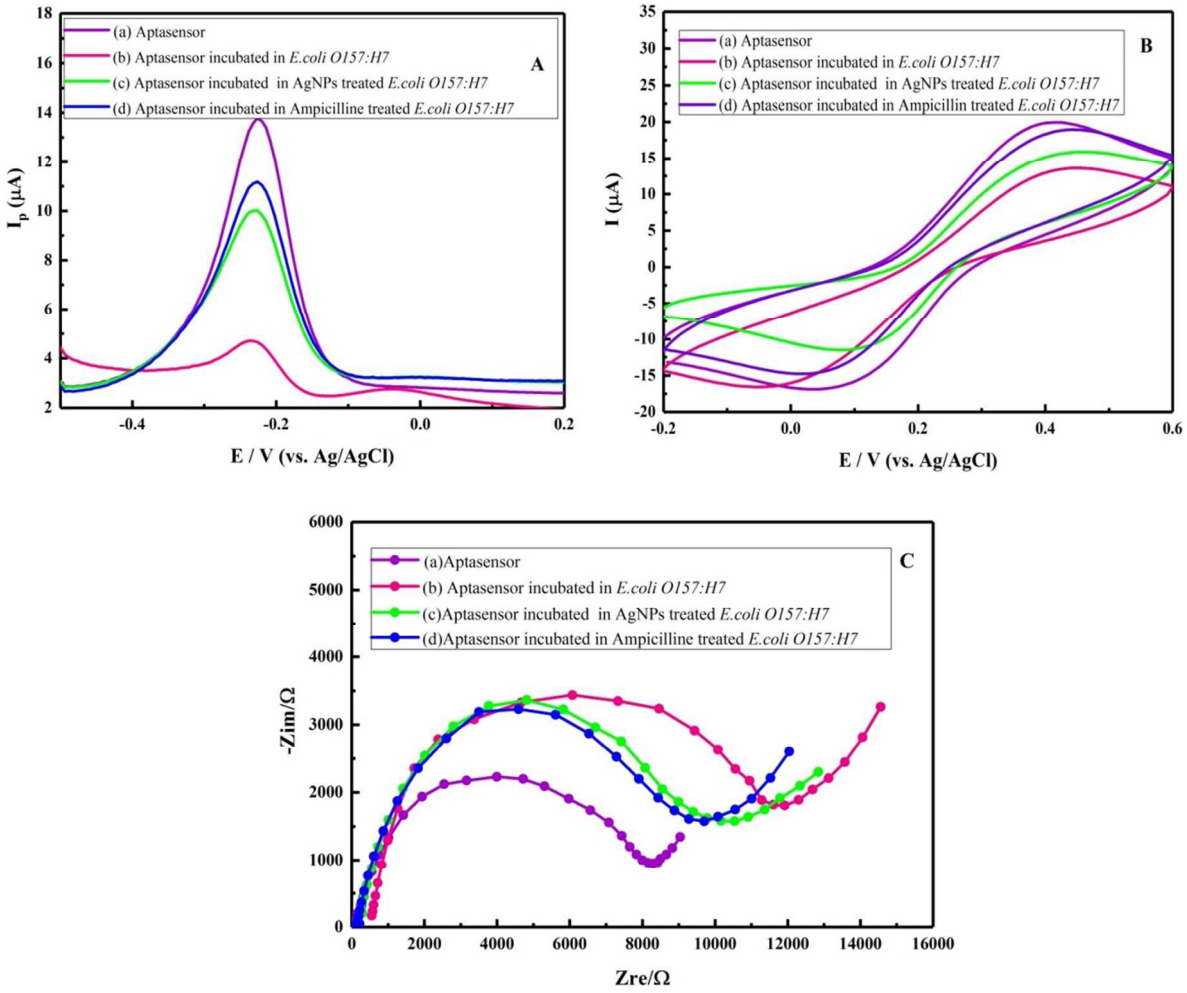

Fig. 6

View Article Online
DOI: 10.1039/C8AN00725J

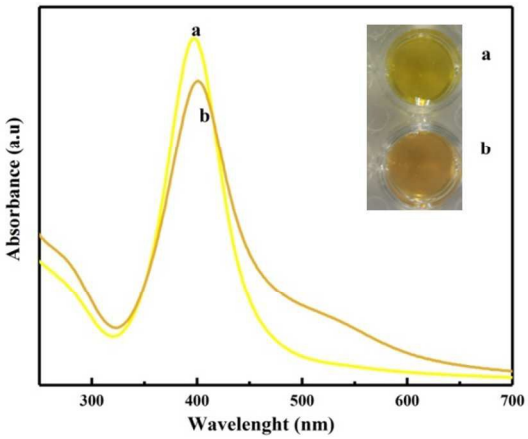

Fig. 7

View Article Online
DOI: 10.1039/C8AN00725J

Graphical Abstract